

Article

Tripling the Optical Efficiency of Color-Converted Micro-LED Displays with Funnel-Tube Array

Fangwang Gou ¹, En-Lin Hsiang ¹, Guanjun Tan ¹, Yi-Fen Lan ², Cheng-Yeh Tsai ² and Shin-Tson Wu ^{1,*}

¹ College of Optics and Photonics, University of Central Florida, Orlando, FL 32816, USA; fangwang.gou@knights.ucf.edu (F.G.); enlinhsiang@gmail.com (E.-L.H.); Guanjun_Tan@knights.ucf.edu (G.T.)

² AU Optronics Corp., Hsinchu Science Park, Hsinchu 300, Taiwan; Even.YF.Lan@auo.com (Y.-F.L.); CY.Tsai@auo.com (C.-Y.T.)

* Correspondence: swu@creol.ucf.edu

Received: 13 December 2018; Accepted: 12 January 2019; Published: 14 January 2019



Abstract: Color-converted micro-LED displays consist of a mono-color micro-LED array and color conversion materials to achieve full color, while relieving the burden of epitaxial growth of three-color micro-LEDs. However, it usually suffers from low efficiency and color crosstalk due to the limited optical density of color conversion materials. With funnel-tube array, the optical efficiency of the color-converted micro-LED display can be improved by ~3X, while the crosstalk is eliminated. After optimization of the taper angle, the ambient contrast ratio is also improved due to higher light intensity.

Keywords: micro-LEDs; color conversion; color crosstalk; ambient contrast ratio

1. Introduction

Micro-LED with a chip size less than 100 μm is a potentially disruptive display technology because of its outstanding features such as low power consumption, good sunlight readability, true black state, high dynamic range and wide color gamut [1–3]. However, it is still challenging for the mass transfer of micro-LEDs from semiconductor wafer to glass substrate with high yield [4,5]. In order to achieve full-color micro-LED displays, several approaches have been proposed. The first method is to grow red, green, and blue (RGB) micro-LEDs on different wafers, and then transfer them to the same TFT-based glass substrates, which requires careful alignment for each pixel. Moreover, the light emission efficiency and degradation rate of RGB micro-LEDs are different; as a result, it may need complicated driving circuit to maintain the color rendering index during operation. The second method is monolithic integration of RGB micro-LEDs via adhesive bonding [6]. However, the fabrication process is complicated, because the substrates for growing blue/green micro-LEDs and red micro-LED are different.

A simpler method to achieve full color is to employ monochromatic UV or blue micro-LEDs together with color conversion materials, such as phosphors or quantum dots (QDs) [7–9]. For example, Han et al. [7] deposited RGB quantum dots on the top of UV LED array by aerosol jet printing method to form individual sub-pixels. This configuration does not need color filters and can achieve high efficiency and wide color gamut. However, for complete color down-conversion, the optical density (OD) of the QDs resin layer must be high, which requires highly absorbing QDs and a relatively thick layer. Therefore, distributed Bragg reflector on the top surface is employed to recycle the UV light and improve the light conversion efficiency of the QDs. A drawback of this approach is the degraded ambient contrast ratio. To solve this problem, another solution is to employ blue micro-LEDs to excite

color conversion materials in order to obtain white light first, and then deposit color filters to achieve RGB subpixels. In this device configuration, the color down-conversion layer does not need to be pixelated, which is more feasible for manufacturing. However, the color filters would absorb 2/3 of the outgoing light. In addition, color crosstalk would occur due to scattering of the color conversion layer.

In this paper, we propose a funnel-tube array for color-converted micro-LED displays in order to reduce color crosstalk and improve light conversion efficiency simultaneously. In addition, the issue of ambient light reflection from the device is addressed.

2. Device Modeling

Figure 1 illustrates the device structures of color-converted micro-LED displays without (device A) and with funnel-tube array (device B), respectively. For device A (Figure 1a), an array of monochromatic blue micro-LEDs with a LED driving backplane are formed on the bottom substrate. Above the micro-LED array, a layer of yellow phosphor is coated to obtain a white light source. On top of the phosphor, a color filter array is used to form RGB subpixels. This system usually suffers from optical color crosstalk, which will be discussed later. To overcome this issue, we propose a funnel-tube array as illustrated in device B (Figure 1b). It is formed above micro-LED layer with the tube region aligned with each subpixel. The inner surface of the funnel-tube can be either absorptive or reflective. The phosphors are filled inside the funnel-tube to obtain white light. On top of the funnel-tube array, the color filters with RGB subpixels are aligned with each tube region. In the system, the phosphors for each subpixel region are designed to be totally isolated. Thus, the color crosstalk will be eliminated.

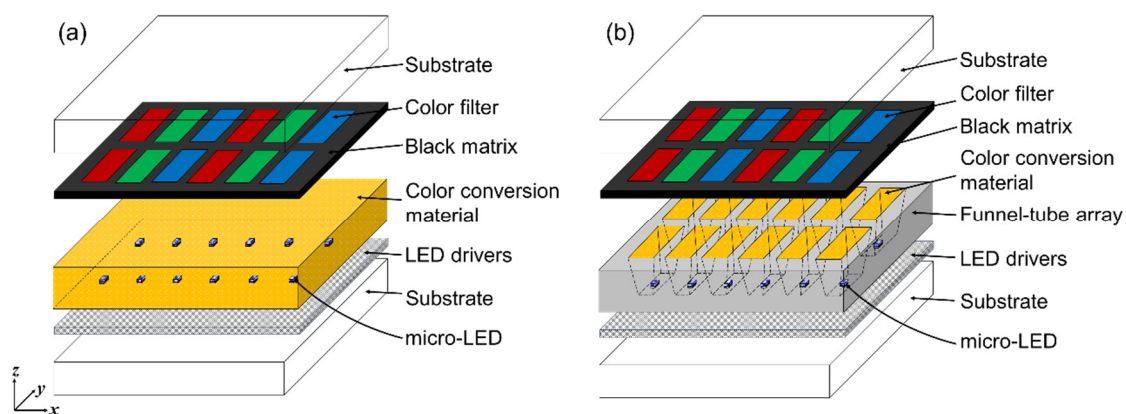


Figure 1. Schematic diagram for configuration of full color micro-LED display (a) device A: without funnel-tube array, and (b) device B: with funnel tube array.

The two display systems are simulated using ray-tracing software LightTools. In our modeling, the display subpixel size is set to be $50\ \mu\text{m} \times 150\ \mu\text{m}$ and the chip size of blue micro-LED is $10\ \mu\text{m} \times 30\ \mu\text{m}$. For simplicity, we assumed that all the micro-LEDs having the same central wavelength of 448 nm with Lambertian angular emission distribution. The phosphor photoluminescence is simulated using LightTools Advanced Physics Module [10,11]. The absorption spectrum, color conversion efficiency, and emission spectrum are all taken into account during calculations (Figure 2a). Because of the small pixel size, the phosphor particle size in the simulation is set to vary from $0.25\ \mu\text{m}$ to $5\ \mu\text{m}$ [12]. The refractive index of phosphor is 1.8 at all wavelengths. The concentration of yellow phosphor is adjusted to obtain a white point for the display system. Simulation process starts with the emission of blue light from the micro-LED array. When the light encountering phosphor particles, the blue light is partially absorbed or scattered by the phosphor particles. The absorbed blue light will be down-converted to yellow light with isotropic radiation, while the scattered light has intensity distributions calculated by Mie theory [10,13]. Re-absorption of yellow light by the phosphor particles is also considered in the modeling. The light emitted from the phosphor will pass through the top color filters following the transmittance spectra shown in Figure 2b [14]. In device A, when only one

micro-LED chip emits light while others remain off, light leakage may come from the surrounding pixels due to the light scattering of the phosphor film, which is referred as color crosstalk. This problem becomes more severe as the thickness of the phosphor film (H) increases [15].

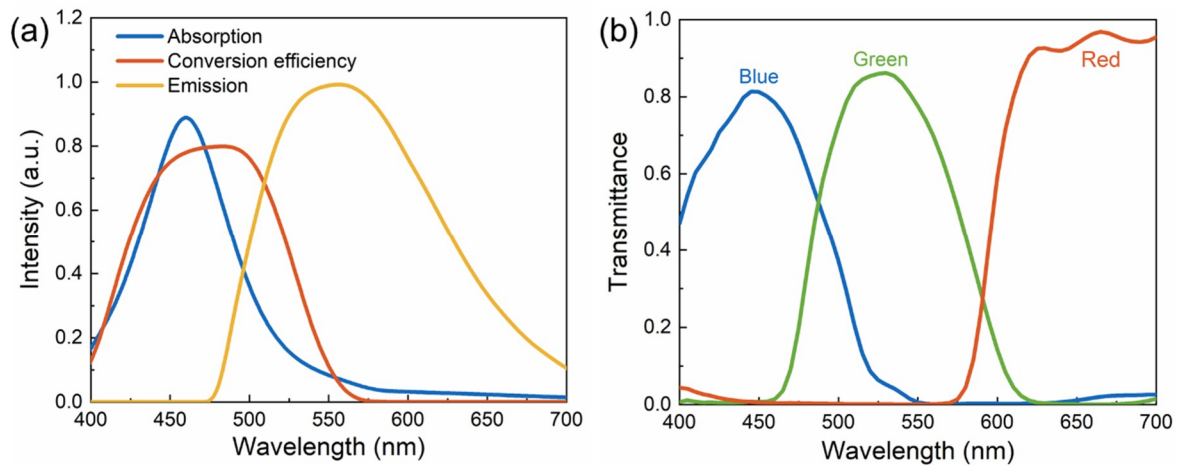


Figure 2. (a) The absorption spectrum, emission spectrum and color conversion efficiency of the employed yellow phosphor. (b) Transmittances of conventional color filters.

3. Simulated Results and Discussion

3.1. Color Crosstalk

To evaluate the color crosstalk quantitatively, two ray receivers with different detection areas were placed above the color filter in our model. Receiver 1 only collected light from one subpixel area ($50 \mu\text{m} \times 150 \mu\text{m}$); the detected light intensity is I_{pixel} . Receiver 2 was able to receive light from the whole panel ($\gg 10$ pixels); the collected light intensity is I_{total} . We defined the color crosstalk ratio as $R_{\text{crosstalk}}$, which can be calculated using Equation (1):

$$R_{\text{crosstalk}} = \frac{I_{\text{leakage}}}{I_{\text{total}}} = \frac{I_{\text{total}} - I_{\text{pixel}}}{I_{\text{total}}} \quad (1)$$

where I_{leakage} represents the light leakage from the adjacent pixels when only one subpixel is turned on. Figure 3 plots the simulated color crosstalk ratio as a function of the phosphor thickness H in device A. As discussed above, when H increases from $15 \mu\text{m}$ to $100 \mu\text{m}$, the optical path inside the phosphor film becomes longer, leading to a more severe light scattering. Therefore, the color crosstalk of RGB subpixels increased accordingly.

Figure 4 shows the simulated color image of device A and device B, respectively. When only one red subpixel was turned on, while green and blue subpixels remained off, the light leakage from the surrounding pixels in device A was severe. In contrast, with the funnel-tube array in device B, no color crosstalk was observed.

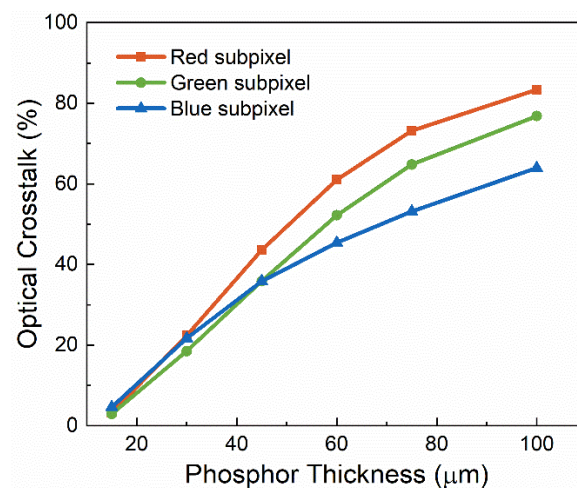


Figure 3. Simulated color crosstalk ratio of device A as a function of phosphor thickness.

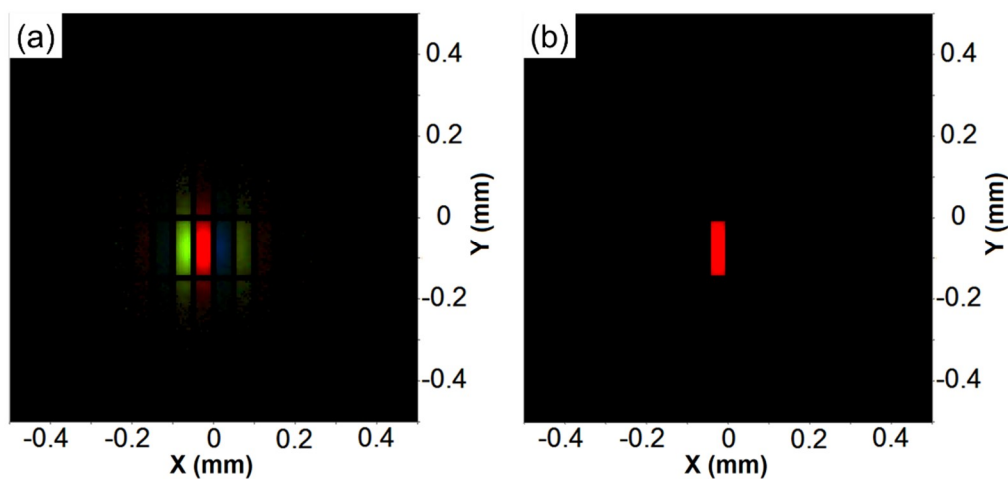


Figure 4. Simulated color images of (a) device A and (b) device B when only one red subpixel is turned on, while green and blue subpixels remain off.

3.2. Light Efficiency and Ambient Contrast Ratio

In order to optimize the performance of the funnel-tube array, we plotted its cross-sectional views in Figure 5. The taper angles of the funnel-tube were α (x - z plane) and β (y - z plane), which could be varied according to the thickness (H), the size of color filter (L_x or L_y) and black matrix (L), and the size of micro-LED (W_x or W_y) as long as the pixels were isolated. In our simulation, we set $W_x = 10 \mu\text{m}$, $W_y = 30 \mu\text{m}$, $L_x = 30 \mu\text{m}$, $L_y = 130 \mu\text{m}$, and $L = 20 \mu\text{m}$. The thickness of funnel-tube was set to be $H = 30 \mu\text{m}$ according to the optical density of the phosphor.

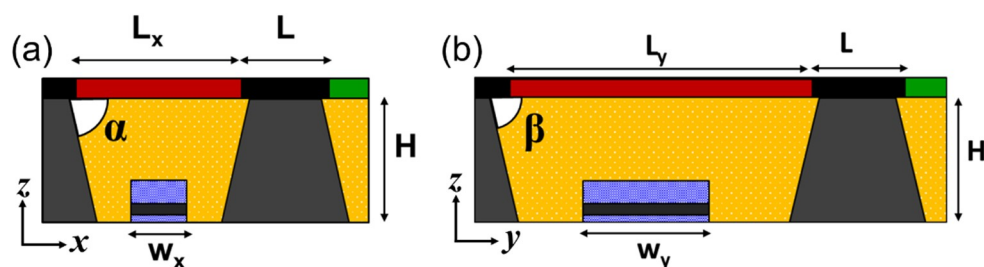


Figure 5. Cross-sectional views of device B in the (a) x - z panel, and (b) y - z plane.

The simulated relative light intensities of device B normalized to that of device A are illustrated in Figure 6. Specifically, in Figure 6a, the taper angle α varied from 72° to 108° , while β was fixed at 37° . In Figure 6b, the taper angle β varied from 31° to 108° when α was set to be 80° . As these figures depict, the light intensity decreased as the taper angle increased. The inner surface of the funnel-tube array contained metallic reflectors to recycle light and elongate the effective optical path inside the phosphors. When the taper angle was larger than 90° , more light was reflected downwards by the inner reflector and then absorbed or scattered by the backplane. On the other hand, when the taper angle was less than 90° , more light was reflected upwards, which then escaped from the device to the air. Therefore, a taper angle less than 90° was preferred to obtain higher light efficiency. However, the ambient light reflection also increased, as illustrated in Figure 6a,b, which would degrade the ambient contrast ratio of the displays. The corresponding relative intensity and ambient reflection are listed in Table 1.

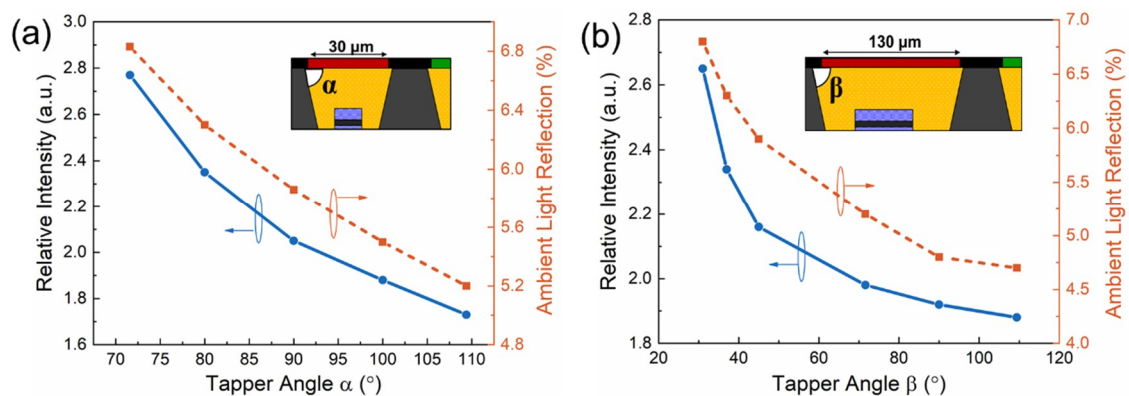


Figure 6. Relative light intensity and ambient light reflection as a function of taper angle (a) α when $\beta = 37^\circ$, and (b) β when $\alpha = 80^\circ$.

Table 1. Relative light intensity and luminous ambient reflection of device B.

| Tapper Angle α ($\beta = 37^\circ$) | 72° | 80° | 90° | 100° | 110° | / |
|--|------------|------------|------------|-------------|-------------|-------------|
| Relative Intensity | 2.77 | 2.35 | 2.05 | 1.88 | 1.73 | / |
| Luminous Ambient Reflection | 6.83% | 6.30% | 5.86% | 5.50% | 5.20% | / |
| Tapper Angle β ($\alpha = 80^\circ$) | 31° | 37° | 45° | 72° | 90° | 108° |
| Relative Intensity | 2.65 | 2.34 | 2.16 | 1.98 | 1.92 | 1.88 |
| Luminous Ambient Reflection | 6.8% | 6.3% | 5.90% | 5.16% | 4.80% | 4.76% |

In order to further understand how the taper angle affects the optical performance, we chose three structures as examples: I ($\alpha = 108^\circ$, $\beta = 108^\circ$), II ($\alpha = 90^\circ$, $\beta = 90^\circ$), and III ($\alpha = 72^\circ$, $\beta = 31^\circ$). The relative light intensities (which were normalized to the light intensity of device A) and ambient luminous reflection of these three structures are listed in Table 2. Compared to device A (without funnel-tube array), the light intensities of structure I, II, and III all improved, indicating higher optical efficiency. Specifically, the light intensity of structure III was $\sim 3X$ larger; however, the luminous ambient light reflection also increased, which would degrade the ambient contrast ratio.

Table 2. Relative light intensity and luminous ambient reflection of structure I, II, and III.

| Structure (α , β) | I (108° , 108°) | II (90° , 90°) | III (72° , 31°) |
|----------------------------------|---------------------------------|--------------------------------|---------------------------------|
| Relative Intensity | 1.22 | 1.53 | 3.02 |
| Luminous Ambient Reflection | 3.28% | 3.94% | 7.07% |

Figure 7 shows the ambient light reflection for RGB subpixels of structure III. The spectral profiles are very similar to the transmittance of color filters (Figure 2b) except for the lower intensity of the blue

light. For the blue subpixel, the blue component of the ambient light transmitted through the color filter and entered the funnel-tube, some of the light was absorbed and then converted by the phosphor, and other light was scattered and reflected inside the funnel tube. A part of the unconverted blue light could escape from the color filter. For green and red subpixels, the ambient light was scattered by the phosphor particles or reflected by the funnel-tube back to the air, leading to higher reflection intensities. Table 3 lists the percentage of ambient light reflection for each subpixel of structure I, II, and III. Due to human eye sensitivity, ambient reflection from green subpixel was dominant.

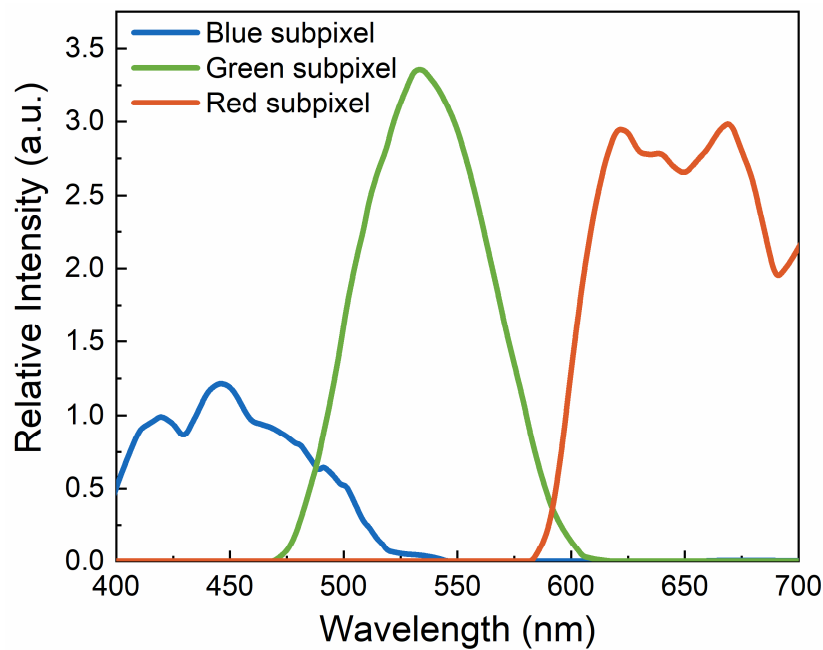


Figure 7. Ambient light reflection for red, green, and blue (RGB) subpixels of structure III.

Table 3. Luminous ambient reflection for RGB subpixels of structure I, II, and III.

| Pixels | RGB | Blue | Green | Red |
|----------------|-------|-------|-------|-------|
| I (108°, 108°) | 3.28% | 0.13% | 2.47% | 0.68% |
| II (90°, 90°) | 3.94% | 0.15% | 2.96% | 0.83% |
| III (72°, 31°) | 7.07% | 0.28% | 5.29% | 1.50% |

The ambient contrast ratio (ACR) of these three structures was calculated using following equation [16,17]:

$$ACR = \frac{L_{on} + L_{ambient} \cdot R_L}{L_{off} + L_{ambient} \cdot R_L} \quad (2)$$

In Equation (2), L_{on} (L_{off}) represents the on-state (off-state) luminance value of a display, $L_{ambient}$ is the ambient luminance, and R_L is the luminous reflectance of the display panel. To calculate ACR, the L_{on} of structure I is typically assumed to be 600 nits, while L_{on} of structures II and III can be calculated according to the relative intensity; the results are 752 nits and 1485 nits, respectively. For all structures, L_{off} is 0, the surface reflection was assumed to be 4%. The calculated ACR of structures I, II, and III are plotted in Figure 8a. As the ambient light got stronger, the ACR decreased dramatically first and gradually saturated. Among these three structures, although structure III had the most severe ambient light reflection, it achieved the largest ACR under different ambient light conditions due to its highest brightness. However, under strong ambient light conditions such as full daylight (~20,000 lux), the ACR of three structures were all $\leq 3:1$ (inset of Figure 8a), which is barely readable under sunlight [18]. This relatively low ACR originates from both light scattering by the phosphor

particles and surface reflection. To improve ACR, anti-reflection (AR) coating with a surface reflection of about 0.2% could be employed [19]; results are shown in Figure 8b. When $L_{\text{ambient}} = 20,000$ lux, the ACR could be improved to $\sim 4:1$. However, when the ambient light continued to get stronger, the light scattering by the phosphor particles dominated and the ACR dropped to below 3:1, indicating the display was hardly readable. A straightforward method to enhance ACR is to employ an absorptive material for the funnel-tube array; however, the trade-off is decreased light efficiency.

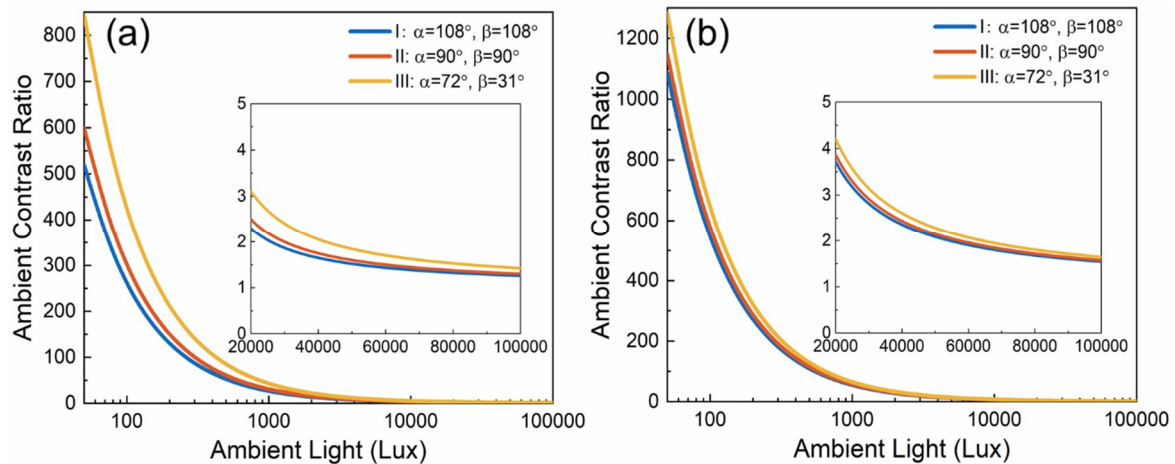


Figure 8. Simulated ambient contrast ratio of structure I, II and III: (a) without AR (anti-reflection) coating (surface reflection $\sim 4\%$), and (b) with AR coating (surface reflection $\sim 0.2\%$).

3.3. Color Gamut

Vivid color is another key metric for display devices, as it enables a more realistic viewing experience. Generally, light sources with a narrower full width at half maximum (FWHM) would lead to a wider color gamut [14]. However, in our modeling, the blue-pumped yellow phosphor converted white light source had a FWHM of about 120 nm, which resulted in limited color gamut. Figure 9 shows the simulated color gamut in CIE 1931 color space for device B with yellow phosphor. This system only covered 78% of DCI-P3 standard [20] and 57% of Rec. 2020 standard [21,22].

In order to improve the color performance, alternative color conversion materials with narrower FWHM can be employed, such as a combination of green phosphor (β -sialon:Eu²⁺, FWHM ~ 50 nm) [23] and red phosphor (K₂SiF₆:Mn⁴⁺) [24], or CdSe red/green QDs (FWHM ~ 25 –30 nm) [25–27]. However, the device structure, especially the thickness of the funnel-tube array, needs to be optimized according to the optical density of the color conversion materials. The simulated color gamut of two-color phosphors and QDs are depicted in Figure 10. The phosphor covered 95% of DCI-P3 standard and 68% of Rec. 2020 standard, and the QDs covers 94% of DCI-P3 standard and 83% of Rec. 2020 standard.

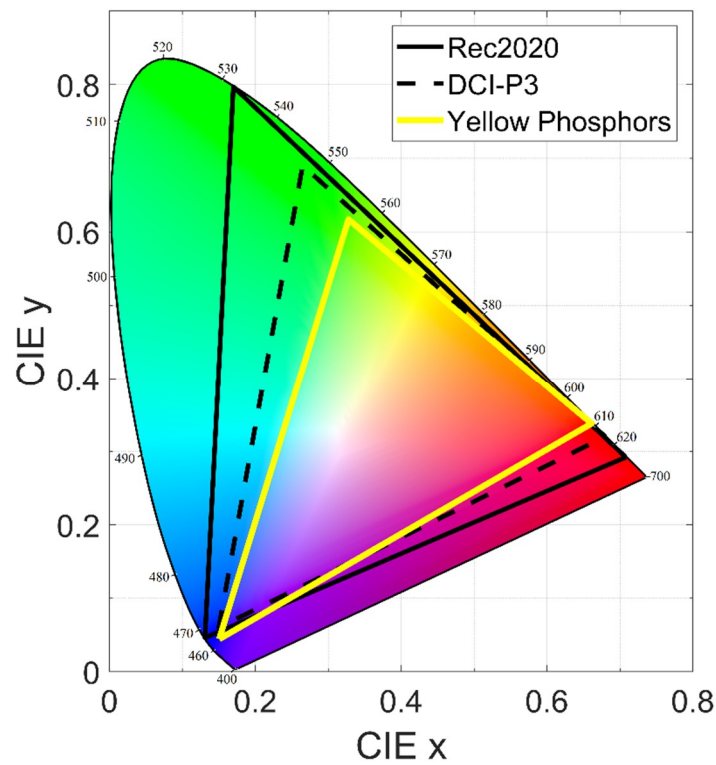


Figure 9. Simulated color gamut for device B with yellow phosphor in CIE 1931 color space.

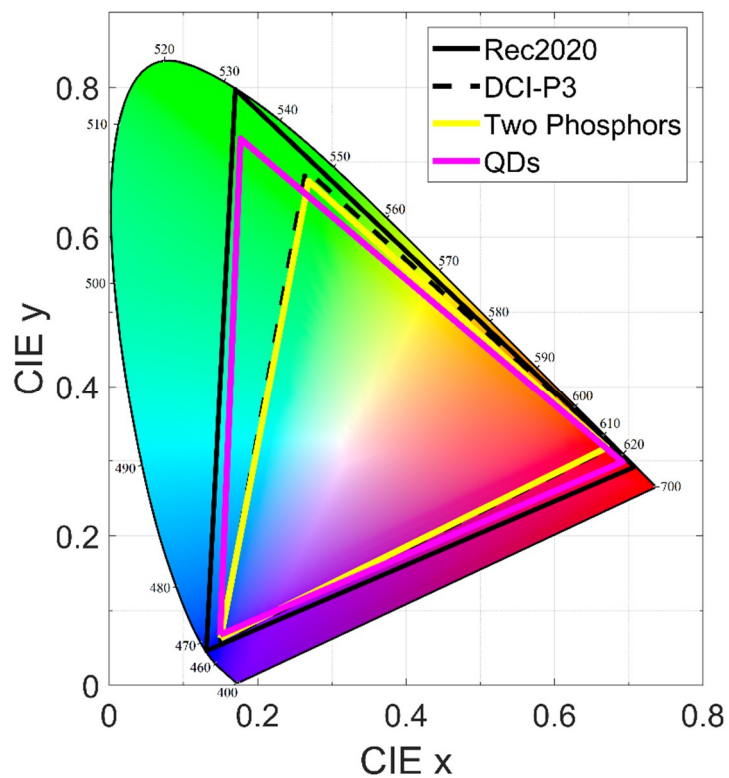


Figure 10. Simulated color gamut for device B with two phosphors (green: β -sialon:Eu⁺, red: K₂SiF₆:Mn⁴⁺) and red/green quantum dots (QDs) in CIE 1931 color space.

4. Conclusions

In this work, we proposed a funnel-tube array to improve the light efficiency and eliminate the color crosstalk of the color-converted micro-LED displays. Based on the simulated results, as the taper angle of the funnel-tube becomes smaller, the light efficiency of the device can be increased by ~3X. Moreover, the ambient contrast ratio was also improved due to higher light intensity, despite the fact that the ambient reflection increased. Despite of the yellow phosphor used in the simulation, our funnel-tube array is also applicable to other color conversion materials, such as green/red phosphors, quantum dots, and perovskites, in order to improve color gamut.

Author Contributions: Conceptualization, F.G. and S.T.W.; methodology, F.G. and G.T.; software, F.G. and G.T.; validation, F.G. and E.L.S.; formal analysis, F.G.; investigation, F.G.; resources, Y.F.L, C.Y.T, and S.T.W.; data curation, F.G. and E.L.S.; writing—original draft preparation, F.G.; writing—review and editing, S.T.W.; visualization, F.G.; supervision, S.T.W.; project administration, Y.F.L, C.Y.T, and S.T.W.; funding acquisition, S.T.W.

Funding: This research was funded by a.u.Vista, Inc.

Conflicts of Interest: The authors declare no conflict of interest.

References

- Jin, S.X.; Li, J.; Li, J.Z.; Lin, J.Y.; Jiang, H.X. GaN microdisk light emitting diodes. *Appl. Phys. Lett.* **2000**, *76*, 631. [CrossRef]
- Jiang, H.X.; Lin, J.Y. Nitride micro-LEDs and beyond—A decade progress review. *Opt. Express* **2013**, *21*, A475–A484. [CrossRef] [PubMed]
- Liu, Z.; Chong, W.C.; Wong, K.M.; Lau, K.M. GaN-based LED micro-displays for wearable applications. *Microelectron. Eng.* **2015**, *148*, 98–103. [CrossRef]
- Virey, E.H.; Baron, N. Status and prospects of microLED displays. *SID Int. Symp. Dig. Tech. Pap.* **2018**, *49*, 593–596. [CrossRef]
- Paranjpe, A.; Montgomery, J.; Lee, S.M.; Morath, C. Micro-LED displays: Key manufacturing challenges and solutions. *SID Int. Symp. Dig. Tech. Pap.* **2018**, *49*, 597–600. [CrossRef]
- Kang, C.-M.; Lee, J.-Y.; Kong, D.-J.; Shim, J.-P.; Kim, S.; Mun, S.-H.; Choi, S.-Y.; Park, M.-D.; Kim, J.; Lee, D.-S. Hybrid full-color inorganic light-emitting diodes integrated on a single wafer using selective area growth and adhesive bonding. *ACS Photonics* **2018**, *5*, 4413–4422. [CrossRef]
- Han, H.-V.; Lin, H.-Y.; Lin, C.-C.; Chong, W.-C.; Li, J.-R.; Chen, K.-J.; Yu, P.; Chen, T.-M.; Chen, H.-M.; Lau, K.-M. Resonant-enhanced full color emission of quantum-dot-based micro-LED display technology. *Opt. Express* **2015**, *23*, 32504–32515. [CrossRef]
- Lin, H.-Y.; Sher, C.-W.; Hsieh, D.-H.; Chen, X.-Y.; Chen, H.-M.P.; Chen, T.-M.; Lau, K.-M.; Chen, C.-H.; Lin, C.-C.; Kuo, H.-C. Optical cross-talk reduction in a quantum-dot-based full-color micro-light-emitting-diode display by a lithographic-fabricated photoresist mold. *Photonics Res.* **2017**, *5*, 411–416. [CrossRef]
- Chen, G.S.; Wei, B.Y.; Lee, C.T.; Lee, H.Y. Monolithic red/green/blue micro-LEDs with HBR and DBR structures. *IEEE Photonics Technol. Lett.* **2018**, *30*, 262–265. [CrossRef]
- Zollers, M. Phosphor modeling in LightTools. LightTools White Paper. 2011. Available online: <http://optics.synopsys.com/lighttools/pdfs/ModelingPhosphorsInLightTools.pdf> (accessed on 24 February 2018).
- Tran, N.T.; You, J.P.; Shi, F.G. Effect of phosphor particle size on luminous efficacy of phosphor-converted white LED. *J. Lightw. Technol.* **2009**, *27*, 5145–5150. [CrossRef]
- Fern, G.R.; Harris, P.G.; Ireland, T.G.; Sliver, J. Sub-micrometre phosphor preparation for next generation displays. *SID Int. Symp. Dig. Tech. Pap.* **2017**, *48*, 1711–1714. [CrossRef]
- Hulst, H.C.; van de Hulst, H.C. *Light Scattering by Small Particles*; Wiley: Hoboken, NJ, USA, 1957.
- Luo, Z.Y.; Chen, Y.; Wu, S.T. Wide color gamut LCD with a quantum dot backlight. *Opt. Express* **2013**, *21*, 26269–26284. [CrossRef] [PubMed]

15. Silver, J.; Harris, P.G.; Fern, G.R.; Bonar, J.; Valentine, G.; Gorton, S. A novel approach to the manufacture of microLED colour conversion structures. In Proceedings of the International Displays Workshop, Fukuoka, Japan, 7–9 December 2016; Available online: <http://bura.brunel.ac.uk/handle/2438/13965> (accessed on 18 April 2018).
16. Dobrowolski, J.A.; Sullivan, B.T.; Bajcar, R.C. Optical interference, contrast-enhanced electroluminescent device. *Appl. Opt.* **1992**, *31*, 5988–5996. [[CrossRef](#)] [[PubMed](#)]
17. Singh, R.; Narayanan Unni, K.N.; Solanki, A. Deepak, Improving the contrast ratio of OLED displays: An analysis of various techniques. *Opt. Mater.* **2012**, *34*, 716–723. [[CrossRef](#)]
18. Walker, G. GD-Itronix Dynavue Technology: The ultimate outdoor-readable touch-screen display. *Rugged PC Rev.* 2007. Available online: http://www.ruggedpcpreview.com/3_technology_itronix_dynavue.html (accessed on 24 July 2017).
19. Tan, G.; Lee, J.-H.; Lan, Y.-H.; Wei, M.-K.; Peng, L.-H.; Cheng, I.-C.; Wu, S.-T. Broadband antireflection film with moth-eye-like structure for flexible display applications. *Optica* **2017**, *4*, 678–683. [[CrossRef](#)]
20. SMPTE RP 431-2. D-Cinema quality—reference projector and environment. 2011. [[CrossRef](#)]
21. ITU-R Recommendation BT.2020. Parameter Values for Ultra-High Definition Television Systems for Production and International Programme Exchange. 2015. Available online: <https://www.itu.int/rec/R-REC-BT.2020/en> (accessed on 03 December 2018).
22. Masaoka, k.; Nishida, Y.; Sugawara, M.; Nakasu, E. Design of primaries for a wide-gamut television colorimetry. *IEEE Trans. Broadcast* **2010**, *56*, 452–457. [[CrossRef](#)]
23. Wang, L.; Wang, X.; Kohsei, T.; Yoshimura, K.; Izumi, M.; Hirotsaki, N.; Xie, R.J. Highly efficient narrowband green and red phosphors enabling wider color-gamut LED backlight for more brilliant displays. *Opt. Express* **2015**, *23*, 28707–28717. [[CrossRef](#)]
24. Adachi, S.; Takahashi, T. Direct synthesis and properties of K₂SiF₆:Mn⁴⁺ phosphor by wet chemical etching of Si wafer. *J. Appl. Phys.* **2008**, *104*, 023512. [[CrossRef](#)]
25. Jang, E.; Jun, S.; Jang, H.; Lim, J.; Kim, B.; Kim, Y. White-light-emitting diodes with quantum dot color converters for display backlights. *Adv. Mater.* **2010**, *22*, 3076–3080. [[CrossRef](#)]
26. Chen, H.; He, J.; Wu, S.T. Recent advances on quantum-dot-enhanced liquid-crystal displays. *IEEE J. Sel. Top. Quantum Electron.* **2017**, *23*, 1900611. [[CrossRef](#)]
27. Zhu, R.; Luo, Z.; Chen, H.; Dong, Y.; Wu, S.T. Realizing Rec. 2020 color gamut with quantum dot displays. *Opt. Express* **2015**, *23*, 23680–23693. [[CrossRef](#)] [[PubMed](#)]



© 2019 by the authors. Licensee MDPI, Basel, Switzerland. This article is an open access article distributed under the terms and conditions of the Creative Commons Attribution (CC BY) license (<http://creativecommons.org/licenses/by/4.0/>).